Bioactive Materials 3 (2018) 110–117

Contents lists available at ScienceDirect

Bioactive Materials

journal homepage: http://www.keaipublishing.com/en/journals/bioactive-materials/

Biodegradation of Mg-14Li alloy in simulated body fluid: A proof-of-concept study

Xiao-Bo Chen [a, b, *], Chuanqiang Li [b, c, d], Daokui Xu [c]

[a] School of Engineering, College of Science, Engineering and Health, RMIT University, Carlton, VIC 3053, Australia
[b] Department of Materials Science and Engineering, Monash University, Clayton, 3800, VIC, Australia
[c] Key Laboratory of Nuclear Materials and Safety Assessment, Institute of Metal Research, Chinese Academy of Sciences, Shenyang, 110016, China
[d] Key Laboratory for Anisotropy and Texture of Materials (Ministry of Education), Northeastern University, Shenyang, 110819, China

ARTICLE INFO

Article history:
Received 14 August 2017
Received in revised form
23 August 2017
Accepted 29 August 2017
Available online 2 September 2017

Keywords:
Biodegradable materials
Magnesium-lithium alloys
MEM
SEM
Potentiodynamic polarisation

ABSTRACT

High corrosion kinetics and localised corrosion progress are the primary concerns arising from the clinical implementation of magnesium (Mg) based implantable devices. In this study, a binary Mg-lithium (Li) alloy consisting a record high Li content of 14% (in weight) was employed as model material aiming to yield homogenous and slow corrosion behaviour in a simulated body fluid, *i.e.* minimum essential medium (MEM), in comparison to that of generic Mg alloy AZ31 and biocompatible Mg-0.5Zn-0.5Ca counterparts. Scanning electron microscopy examination reveals single-phase microstructural characteristics of Mg-14Li (β-Li), whilst the presence of insoluble phases, cathodic to α-Mg matrix, in AZ31 and Mg-0.5Zn-0.5Ca. Though slight differences exist in the corrosion kinetics of all the specimens over a short-term time scale (no longer than 60 min), as indicated by potentiodynamic polarisation and electrochemical impedance spectroscopy, profound variations are apparent in terms of immersion tests, *i.e.* mass loss and hydrogen evolution measurements (up to 7 days). Cross-sectional micrographs unveil severe pitting corrosion in AZ31 and Mg-0.5Zn-0.5Ca, but not the case for Mg-14Li. X-ray diffraction patterns and X-ray photoelectron spectroscopy confirm that a compact film (25 μm in thickness) consisting of lithium carbonate (Li_2CO_3) and calcium hydroxide was generated on the surface of Mg-14Li in MEM, which contributes greatly to its low corrosion rate. It is proposed therefore that the single-phase structure and formation of protective and defect-free Li_2CO_3 film give rise to the controlled and homogenous corrosion behaviour of Mg-14Li in MEM, providing new insights for the exploration of biodegradable Mg materials.

1. Introduction

Biodegradable magnesium (Mg) and its alloys are promising materials candidate for implantable devices, where mechanical strength and biological functions are expected over a certain time length, such as screws, pins and plates in bone fracture management [1,2]. One of the dominant hindrances for the commercial employment of Mg-based implant devices is ascribed to their rapid *in vivo* degradation process, which can deteriorate mechanical integrity significantly and reduce the desired lifespan to a great magnitude [3,4]. The degradation products, including insoluble metal oxide/phosphates, hydrogen gas, and soluble Mg^{2+} and hydroxyl (OH^-) ions, can incur a number of detrimental reactions to the surrounding tissues and matrices [5,6].

To regulate the high degradation kinetics of Mg and its alloys, a variety of feasible strategies have been developed [7,8]. Barrier coatings can isolate the underlying Mg implants from aggressive environments to yield a low degradation rate (down to approx. 0.1 mg/cm^2/day) [9]. However, when the protective function of the coatings elapses with exposure time to the physiological environments, high degradation kinetics will be triggered to release toxic/unfavourable ingredients to immediate regions [2,10]. In addition, microstructural controls through alloying Mg matrix with one or more biocompatible elements could reduce the degradation kinetics of yielded Mg alloys [3,11,12].

* Corresponding author. School of Engineering, College of Science, Engineering and Health, RMIT University, Carlton, VIC 3053, Australia.
E-mail address: xiaobo.chen@rmit.edu.au (X.-B. Chen).
Peer review under responsibility of KeAi Communications Co., Ltd.

http://dx.doi.org/10.1016/j.bioactmat.2017.08.002

In this regard, two key hypotheses were postulated to regulate the rapid degradation behaviour of Mg alloys. From metallurgical perspectives, alloying elements, such as zirconium (Zr) and strontium (Sr), have been broadly employed to modify the microstructure for refined grain size, narrow size distribution and mitigated degradation rate [13,14]. The other option is to change the bulk materials by means of addition of zinc (Zn) into Mg matrix, aiming to alleviate the degradation kinetics through the formation of a native and protective film consisting of ZnO_2 on the surface of Mg-Zn alloys [12,15], a feasible strategy analogous to that of chromium containing stainless steels. Though the microstructural modifications (either metallurgical or chemical) impose significant controls over degradation of Mg, the reported results are still far from the basic requirements for clinical uptakes. As such, after years of extensive studies of the tactics to yield Mg alloys for biomedical applications, commercial success in Mg-based implantable products remains rare. Moreover, as far as the safety concerns, the options of alloying elements for biomedical uses are limited to calcium (Ca), Zn, Sr, manganese (Mn) and a small variety of rare earth elements [3].

Lithium (Li) is an emerging option to preserve or enhance bone mineral density [16], and demonstrate an anabolic effect on bone mass in mice [17]. Li has been incorporated to bone filler materials (*i.e.* 45S5 bioglass and hydroxyapatite) to increase their therapeutic properties [18]. In terms of Mg alloys, Li is a beneficial alloying constituent to formability and duplex structures, but a potent accelerator for corrosion, owing to its high electrochemical and chemical activity [19–22]. It has been widely recognised that the corrosion rate of Mg-Li alloys increases as a function of concentration of Li in Mg. In late 2015, Xu and colleagues reported that an addition of Li up to 10.3 wt% (approx. 33 at%) can retain its beneficial role in ductility and strength, and amazingly reduce the corrosion rate, which outperforms most existing Mg alloys [23]. Such a remarkable corrosion resistance of Mg-Li alloy is attributed to the formation of a protective lithium carbonate (Li_2CO_3) film on the surface [23,24] with exposure to air or carbonated NaCl environments. It, therefore, inspires the present study to investigate the feasibility of addition of Li to Mg matrix as next generation biodegradable materials with satisfactory degradation profile through the formation of Li_2CO_3 in the carbonate-rich physiological environments.

In this proof-of-concept study, a binary Mg-14Li (wt%, equivalent to 36.3 at%) was prepared to elucidate the formation mechanism of the surface coatings and their role in regulating degradation of the underlying Mg-Li alloy in a carbonate-rich simulated body fluid, *i.e.* minimum essential medium (MEM), with two generic biocompatible Mg alloys (Mg-0.5Zn-0.5Ca and Mg-3Al-1Zn, both in wt.%) as negative controls. Surface and cross-sectional morphology, chemical and crystallographic composition (prior to and after immersion in MEM), degradation profiles are characterised through scanning electron microscopy (SEM), X-ray photoelectron spectroscopy (XPS) and diffraction (XRD), potentiodynamic polarisation and electrochemical impedance spectroscopy (EIS), mass loss and hydrogen evolution, respectively. It is anticipated to provide a new knowledge paradigm to guide the design and manufacturing of biodegradable Mg alloys to satisfy the requirements for implantable devices.

2. Materials and methods

2.1. Materials preparation

Commercial AZ31 plats were supplied by School of Materials Science and Engineering, Chongqing University, China with a chemical composition of 3.46% Al, 0.93% Zn, 0.31% Mn, 0.02% Fe, and bal. Mg (in wt.%). Mg-0.5Zn-0.5Ca (wt.%) was prepared by induction melting 99.9 wt% pure Mg (≤40 ppm Fe) (AMAC, Australia) with pure Zn (99.9%) (Alfa Aesar, USA) and Mg-28Ca (wt.%) master alloy (Alfa Aesar, USA), in a graphite coated steel crucible under the protection of argon atmosphere. Mg-14Li alloy (wt%) was melted with commercial pure Mg (99.9 wt%) and Li (99.9 wt%) in a vacuum induction furnace under protection of argon gas.

Raw Mg, and Mg-28Ca pieces were stored in cool, dry wooden containers, whilst the as-prepared alloy specimens were stored in vacuum desiccators to avoid contamination and oxidation (corrosion). To avoid oxidation and ignition of molten Mg, furnace chamber was evacuated down to ~10^{-2} bar and filled with argon gas. All apparatus that contacted with the molten Mg, including stirrer, thermocouple protector and mould, were coated with graphite to minimise Fe contamination. The mixture of metals was heated up to 720 °C at a rate of 3–5 °C s^{-1} and maintained for 25–30 min, with vigorous stirring every 5 min. The melt was then poured into a rectangular mould preheated to 200 °C to reduce shrinkage, followed by cooling down to room temperature at an average rate of 1 °C s^{-1}.

Regarding Mg-Li alloy production, the raw materials were loaded in a graphite crucible and the furnace chamber pressure was maintained at 1 × 10^{-2} Pa and heated up till metal liquid was generated. Subsequently, metal melt was slowly transferred into a 280-mm high cone-shaped iron mould with a diameter of 90 mm at one side and 110 mm at the other size. Afterwards, the ingots were machined to a standard column with the dimension of Φ80 mm × 260 mm. Finally, the machining ingot was extruded into thick plates with a rectangle outlet with dimensions of 50 mm × 16 mm at 300 °C to yield an extrusion ratio of 6.3 to minimise the intrinsic defects, refine the grains and mechanical strength of ingots produced by casting process.

2.2. Microstructural evaluations

Scanning electron microscopy (SEM) was conducted using a JEOL 7001F equipped with a Bruker energy dispersive X-ray spectroscopy (EDX) system. For cross-sectional observations, the specimens were cold mounted with epoxy and sectioned in middle. To retrieve cross-sectional regions, specimens were grounded progressively down to 2000 grit finish with silicon carbide papers, followed by polishing with 3 and 1 μm diamond paste prior to final polishing with 0.5 μm colloidal silica suspension to obtain a mirror-like surface finish. The polished specimens were then chemically etched using a picric acid solution to reveal microstructures. Crystallographic study of the as-prepared alloys prior to and after immersion tests was conducted using X-ray diffraction (XRD; Philips PW1140) under the condition of CuK_α radiation (λ = 1.5418 Å), 40 kV and 25 mA at a scanning speed of 0.5 °C min^{-1} between 10 and 80°. X-ray photoelectron spectroscopy (XPS; Thermo K-alpha) was performed with a hemispherical “analyser” to reveal surface chemistry of the specimens prior to and after immersion tests. In addition to general survey, the core level XPS spectra for Mg 2p, Li 1s, Ca 2p, Zn 2p, P 2p, O 1s and C 1s were recorded. The measured binding energy values were calibrated by C1s (hydrocarbon C–C, C–H) of 285 eV. Photoelectrons were generated by Al K_α (1486.6 eV) primary radiation (20 kV, 15 mA).

2.3. Electrochemical study

Electrochemical tests were performed using a flat cell (EL-FLAT_3, Bio-Logic®) containing 300 ml MEM at 37 °C and pH 7.4 ± 0.4. The cell was designed with a double jacket for delicate temperature control and three pinholes to accommodate reference electrode, purge tube and temperature probe. Potentiodynamic

polarisation tests were carried out at a scan rate of 1 mV s^{-1} after 10 min open circuit potential (OCP) conditioning. Corrosion current density (i_{corr}) and corrosion potential (E_{corr}) were estimated by linear Tafel fitting the polarisation curves using EC-Lab software (version 11.12, BioLogic®). Polarisation curves provide kinetics of anodic and cathodic reactions of the tested samples, which can be applied to interpret their corrosion mechanisms. Electrochemical impedance spectra (EIS) tests were conducted over the frequency range of 100 kHz to 10 mHz. The EIS spectra were fitted using EC-Lab software (version 11.12, BioLogic®). A minimum of ten replicates were taken for each specimen for reproducibility.

2.4. Immersion tests

Alloy samples were cut into cubic shapes of 5 mm in each dimension and ground to a 2000 grit SiC paper finish for hydrogen evolution and mass loss testing, performed in minimum essential medium (MEM, Invitrogen) in a sterile Sanyo incubator at constant temperature of 37 °C in a humidified atmosphere containing 5% CO_2. The samples were ultrasonically cleaned in ethanol in for 3 min prior to immersion in MEM. A constant ratio of volume of MEM to sample area of 150 ml cm^{-2} was employed to minimise the influence of pH and ionic strength variation. pH value was 7.4 at the beginning of immersion and the MEM solution was refreshed every 2 days to maintain the ion concentrations (and bulk pH). Hydrogen volume evolved during MEM immersion was collected using a funnel placed over the specimen. A burette was mounted over the funnel and filled with MEM. The connections of funnel-burette and burette-peleus ball were sealed using Para film to avoid leakage.

After immersion for 3 and 7 days, respectively, samples were removed from MEM solution and cleaned using 200 g l^{-1} of chromic acid and 10 g l^{-1} $AgNO_3$ at room temperature for 1 min according to the ASTM G1-03 standards to remove corrosion products, followed by drying in air [25]. The weight of each specimen was carefully measured before and after immersion to determine a mass loss/degradation rate over different time durations. The mass loss was recorded as degradation rate in a unit of mg day^{-1} cm^{-2} and mean values were obtained from five replicate experiments.

3. Results and discussion

Microstructural characteristics and crystallographic phases of the selected Mg alloys, *i.e.* Mg-0.5Zn-0.5Ca, AZ31 (Mg-3Al-1Zn) and Mg-14Li (all in wt%), were examined through SEM (via backscattered electron mode) and XRD. According to the phase diagram of Mg-Zn-Ca system, Zn and Ca could completely dissolve in Mg matrix to form a solid solution below their maximum solubility limits (Zn 6.2% and Ca 1.8%) [26]. However, in practice, it is difficult to yield such an ideal solid solution of Mg with Zn (0.5 wt%) and Ca (0.5 wt%) and thus insoluble phases, such as $Ca_2Mg_6Zn_3$ and $Mg_{17}Al_{12}$ (XRD patterns in Fig. 1), are apparently scattered in between α-Mg grains (top row in Fig. 1). Given the large difference in corrosion potential of α-Mg matrix and such insoluble phases, numerous micro-galvanic couples (anode: α-Mg; cathode: Al/Zn) exist and accelerate the corrosion kinetics of Mg alloys. Such heterogeneous electrochemistry across the surface of Mg alloys is favourable for localised corrosion, which will deteriorate the mechanical integrity of Mg implants and incur sudden mechanical fractures, a disaster associated with load-bearing components [27]. To control the *in vitro* and *in vivo* degradation progress of Mg implants, micro-galvanic couples should be avoided or minimised through micro-alloying [12] or surface modification strategies [2,9]. In contrast, homogenous and slow corrosion behaviour is anticipated in Mg-14Li owing to the presence of single phase, termed β-Li (Fig. 1), which is a solid solution of Li in body-centred cubic Mg

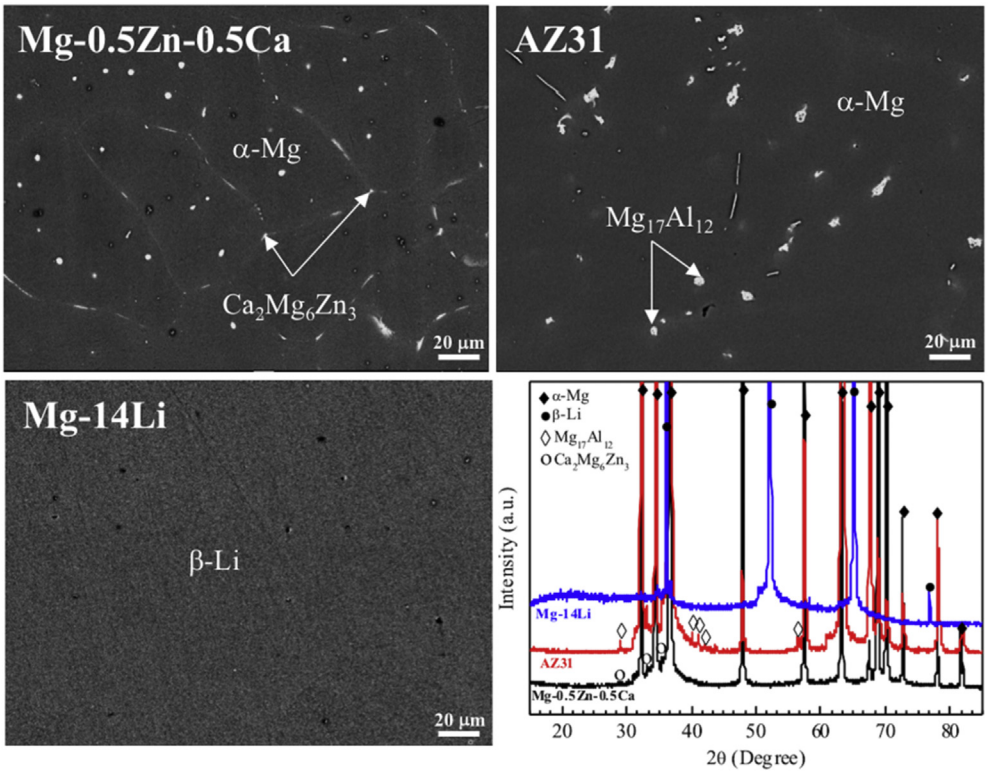

Fig. 1. SEM micrographs of the surfaces and XRD patterns of as-polished Mg alloys Mg-0.5Zn-0.5Ca, AZ31 and Mg-14Li.

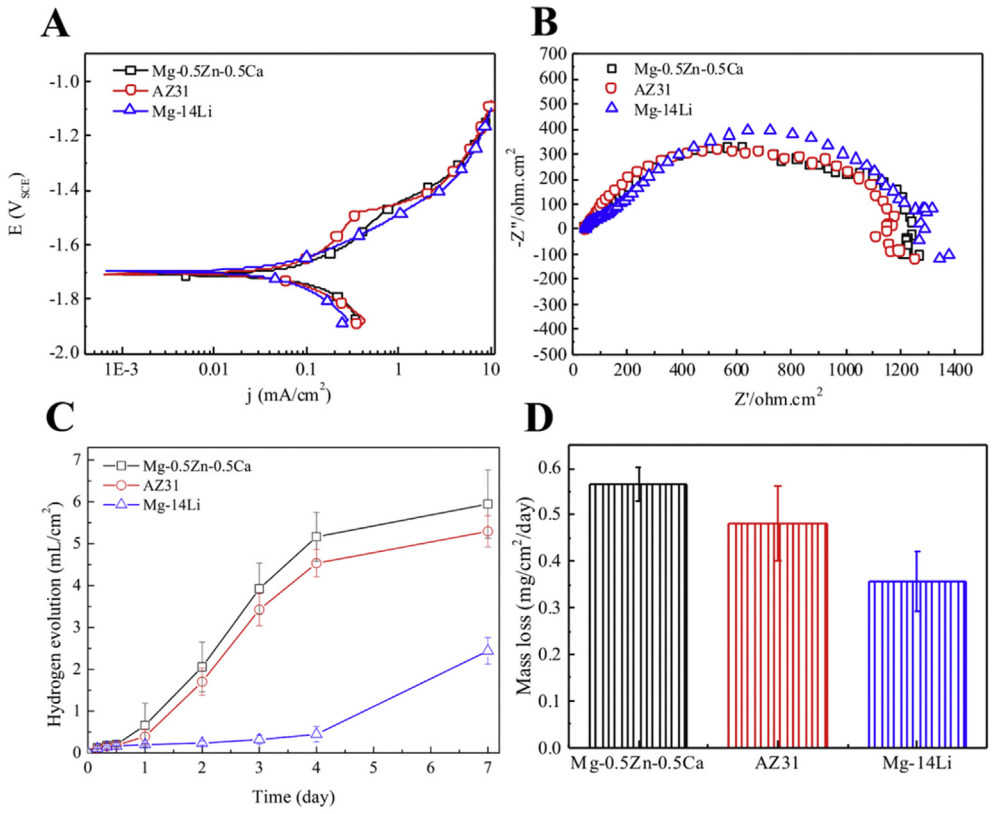

Fig. 2. Degradation characterisations of Mg alloys Mg-0.5Zn-0.5Ca, AZ31 and Mg-14Li in MEM solutions at physiological conditions (37 °C, 5% CO_2 and 95% humidity atmosphere). (A) Potentiodynamic polarisation curves; (B) EIS spectra; (C) Average hydrogen evolution volume as a function of immersion time periods; and (D) Average mass loss after 7 days immersion in MEM. Replicate tests were conducted for each measurement ($n \geq 5$).

matrix and the high tendency to form a protective Li_2CO_3 film on the surface of Li-containing Mg alloys [23].

Instant corrosion kinetics and film formation on the surface of Mg alloys upon in contact with MEM were examined through potentiodynamic polarisation and EIS (top row in Fig. 2), respectively. After 10-min stabilisation at OCP, the anodic and cathodic kinetics of all tested specimens proceeded in a similar manner, though a more obvious passivation is detected on the anodic branch of AZ31, indicating limited passivation derived from the formation passive Al_2O_3 film [8,28]. Slight differences are recorded in EIS plots, revealing the comparative electrochemical reactions on the surfaces of all Mg alloys in MEM over short immersion time lengths (no longer than 60 min). Immersion tests were employed in MEM up to 7 days aiming to reveal the corrosion progress of the Mg alloys over long time scales (bottom row in Fig. 2). It is noted that hydrogen gas was evolved for all cases as a function of immersion time in MEM. The Mg alloys exhibiting heterogeneous structures, *i.e.* Mg-0.5Zn-0.5Ca and AZ31, experienced a steep increase in hydrogen evolution (approx. 5 mL/cm^2 on day 4) and slightly slow down after 4 days. Regarding Mg-14Li, the hydrogen evolution was significantly inhibited (less than 0.5 mL/cm^2 on day 4), which is ascribed partially to its single-phase structure. A similar finding is noted in terms of mass loss measurements.

Cross-sectional micrographs of the Mg alloys specimens were taken to illustrate the development of corrosion pits from the top surface inwards with immersion time in MEM (Figs. 3–6). As anticipated, Mg-0.5Zn-0.5Ca containing a large fraction of $Ca_2Mg_6Zn_3$ phases along the boundary of α-Mg grains is favourable for localised corrosion or pitting corrosion. Corrosion took place at the particular sites (normally α-Mg) with high kinetics and produced deep pits that were filled with corrosion products consisting of profound cracks (after 3 days' immersion in MEM, Fig. 3). AZ31 is also vulnerable to pitting corrosion, though the depth is smaller than that of Mg-0.5Zn-0.5Ca after 3 days' immersion (Fig. 4). Mg-14Li exhibits outstanding corrosion performance in a slow and homogenous way (Fig. 6). No pits are apparent through cross-sectional observations. A thick (approx. 25 μm), compact and defect-free layer containing corrosion products was generated with immersion time in MEM, which contributes greatly to the homogenous corrosion and low corrosion rate of Mg-14Li.

XRD patterns of the Mg alloy specimens (Fig. 7) illustrate that new phases emerged in MEM with time on the surface of Mg-14Li, which are identified as Li_2CO_3 and $Ca(OH)_2$, in addition to β-Li from the underlying substrate. In contrast, XRD patterns of Mg-0.5Zn-0.5Ca and AZ31 exhibit slight differences with immersion proceeding in MEM, indicating a soluble nature of the corrosion products, which provides mild or little protection against future corrosive attacks in MEM. The presence of Li_2CO_3 and $Ca(OH)_2$ in the surface film of Mg-14Li is confirmed through XPS analysis (Table 1), which is the other key contribute to the low degradation rate of Mg-14Li specimens in MEM [23]. $Ca(OH)_2$ is a common degradation by-product of Mg alloys in MEM, where Ca^{2+} and OH^- ions can form insoluble precipitates.

4. General discussion

Low degradation rates and homogenous degradation behaviour are required for Mg-based implants to perform the expected mechanical and biological functions of Mg implants [1,9]. In brief, numerous studies reported that rapid degradation process of Mg gives rise to excess hydrogen gas bubbles, highly alkaline environments and release of a great quantity of metal ions, which could

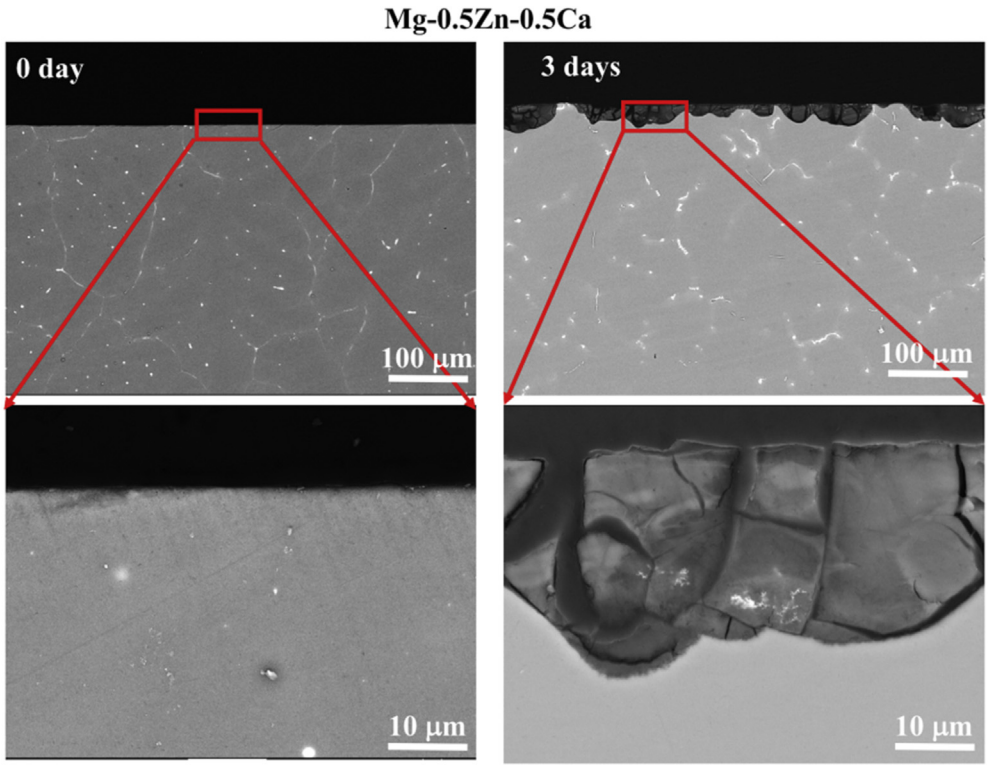

Fig. 3. Cross-sectional SEM micrographs of Mg alloy Mg-0.5Zn-0.5Ca after immersion in MEM for 0 and 3 days, respectively. Detailed features of the rectangle regions in the top row were magnified and provided in the bottom row.

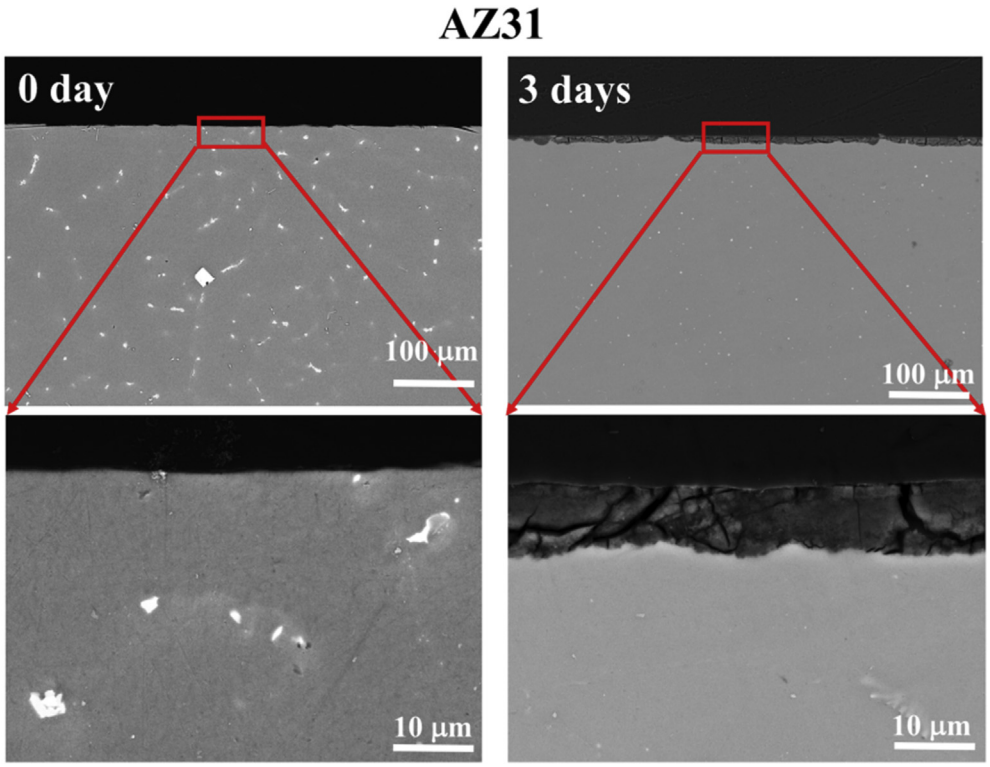

Fig. 4. Cross-sectional SEM micrographs of Mg alloy AZ31 after immersion in MEM for 0 and 3 days, respectively. Detailed features of the rectangle regions in the top row were magnified and provided in the bottom row.

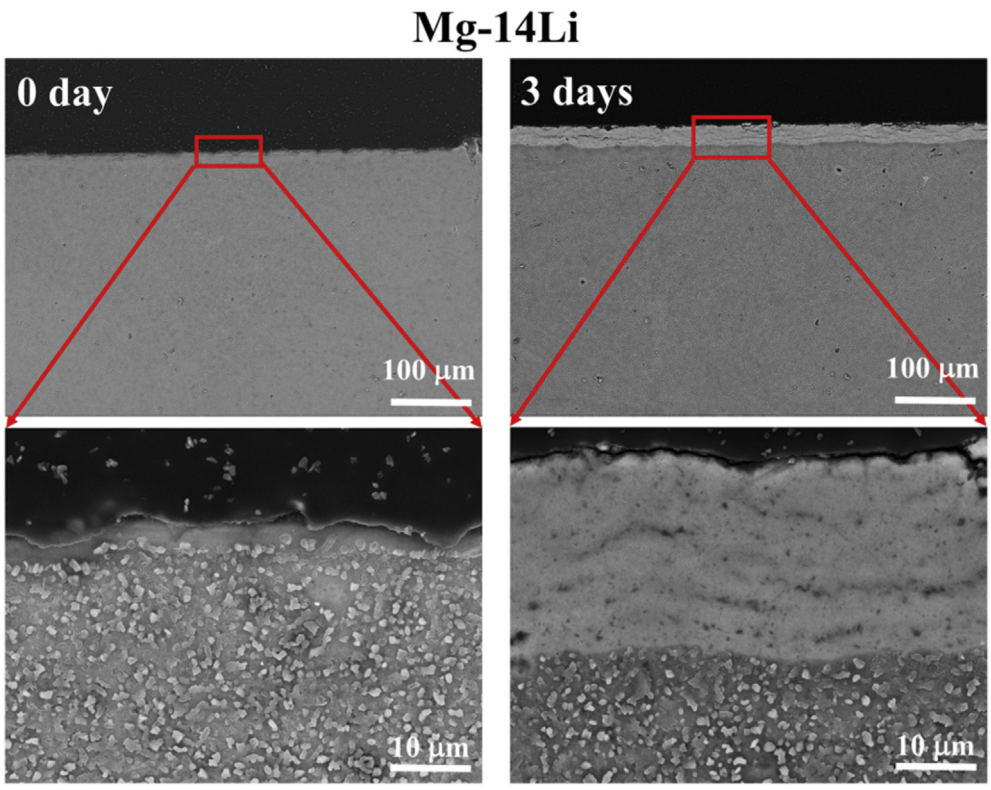

Fig. 5. Cross-sectional SEM micrographs of Mg alloy Mg-14Li after immersion in MEM for 0 and 3 days, respectively. Detailed features of the rectangle regions in the top row were magnified and provided in the bottom row.

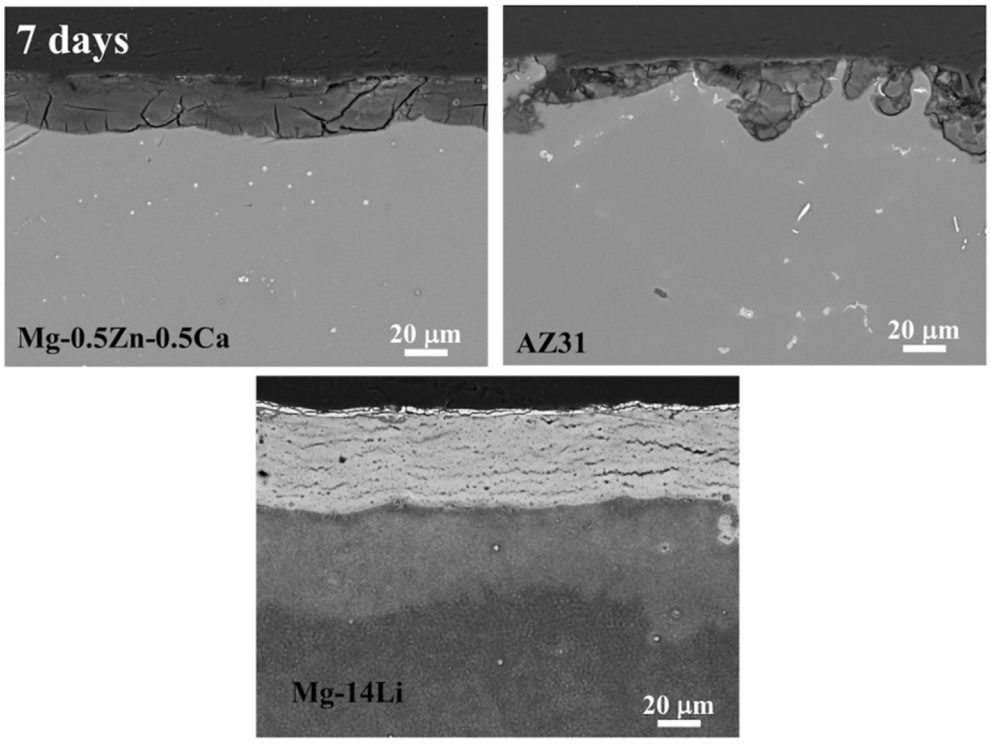

Fig. 6. Cross-sectional SEM micrographs of Mg alloy Mg-0.5Zn-0.5Ca, AZ31 and Mg-14Li after immersion in MEM for 7 days.

kill the cells *in vitro* and trigger infections to the surrounding tissues *in vivo* [29]. Localised or pitting corrosion, will deteriorate the mechanical integrity of structural metal components and incur catastrophic consequences [30].

To address the issues blocking the clinical employment of degradable Mg implants, we hypothesised herein that a complete

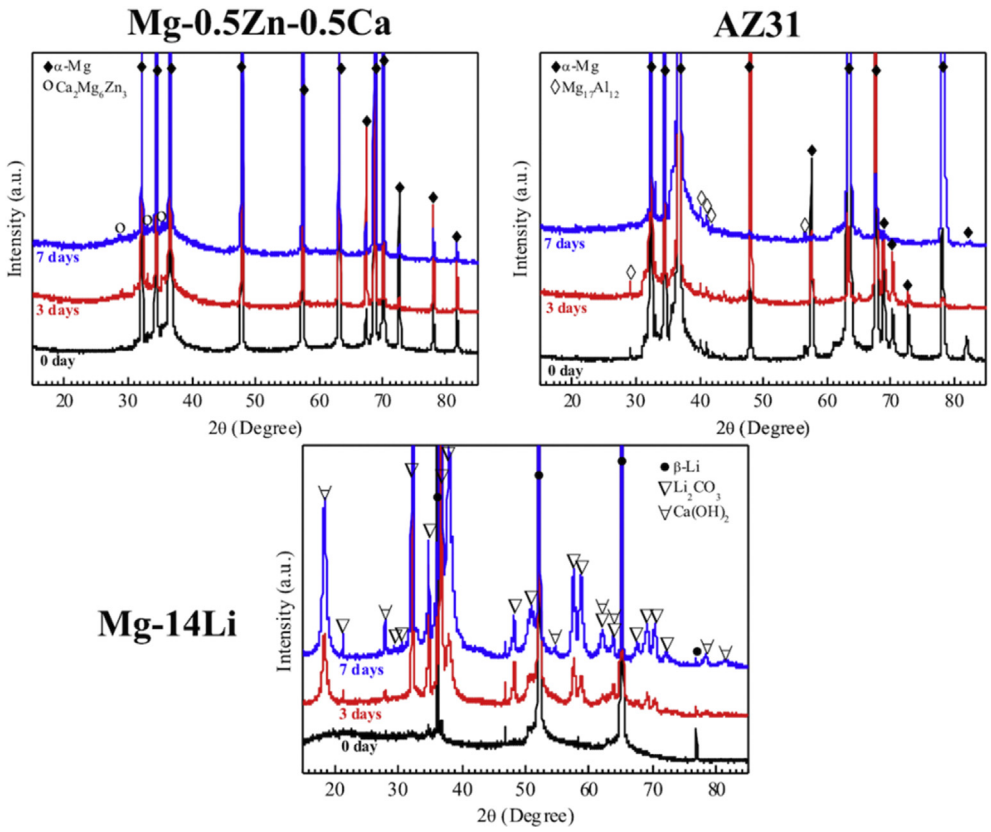

Fig. 7. XRD patterns of the Mg alloy specimens were plotted as a function of immersion time durations from 0 day to 7 days in MEM. The phases were identified according to standard records of JCPDS data base.

Table 1
XPS spectra of the surface of Mg-14Li specimens as a function of immersion time durations from 0 day to 7 days in MEM.

Immersion time (day)	Binding energy of elements (keV) and atomic fractions (at%)					
	Mg 2p	Li 1s	Ca 2p	C 1s	O 1s	P 2p
0	55.58	55.64	–	289.18, 290.48	532.18	–
3	55.51	55.53	347.31	288.78, 290.22	531.92	133.65
7	55.58	55.38	347.29	288.28, 289.68	531.28	133.98

solid solution of Li in Mg matrix would form a homogeneous microstructure (*i.e.* β-Li - homogenous degradation) and yield a highly protective Li_2CO_3 film through subsequent exposure to carbonate-rich physiological media (slow degradation rates), such as MEM. It had been recognised that the addition of Li in Mg matrix accelerates corrosion to a great degree, though it is beneficial to mechanic properties and weigh reduction. The increase in corrosion rate of Mg-Li alloys was a function of the concentration of Li in Mg [31]. In 2015, Xu and his colleagues proposed an opposite theory that addition of excess Li (up to 10.3 wt%) could slow down the corrosion kinetics of Mg through the formation of a passive Li_2CO_3 film upon the exposure to CO_2 in ambient air [23]. More remarkably, the consumption of such protective Li_2CO_3 film can be replenished through the reaction between Li and surrounding CO_2 or carbonate molecules, termed as "self-healing". A following study monitored the corrosion progress of Mg-10.3Li alloy in NaCl through on-line ICP elemental analysis and reported that the Mg-Li alloy dynamically formed a Li-rich persistent surface film that rapidly developed as a result of alloy dissolution [24].

Apart from the existing research, we focused on the degradation behaviour of a binary Mg-Li alloy exhibiting single β-Li phase and record high centration of Li (14 wt%) in MEM over a long term (up to 7 days). It was anticipated such structural features could contribute to a desirable degradation profile that would guide design and manufacturing of implantable Mg devices for future biomedical applications. The microstructural examination (Fig. 1) reveals a single-phase feature of Mg-14Li, which is ascribed to the high solid solubility of Li in α-Mg matrix [19–21]. In contrast, even a small concentration of the alloying elements of Zn and Ca (Mg-0.5Zn-0.5Ca), far below their corresponding solubility thresholds, gives rise to the formation of nobler phases ($Ca_2Mg_6Zn_3$) with respect to α-Mg matrix. The following immersion tests in MEM up to 7 days demonstrate significant differences in the degradation progress of single-phased (Mg-14Li) and multi-phased (Mg-0.5Zn-0.5Ca and AZ31) Mg alloys (Figs. 2–3).

Cross-sectional micrographs (Figs. 4–6) unveil that severe pitting corrosion takes place on the surface of Mg alloys Mg-0.5Zn-0.5Ca and AZ31 and proceeds deeply downwards to the centre of the metal specimens. It is anticipated that mechanical integrity, in terms of tensile strength, ductility and fatigue resistance, will be jeopardized exponentially with immersion time. When the load-bearing bone sites are substituted with Mg components, localised corrosion will generate great concerns over safety and functional lifespan. Regarding temporary implants, degradation is desired (to

eliminate secondary removal surgery) as long as it proceeds with a slow rate and follow a predictable pathway. The latter is critically associated with homogenous degradation, analogous to that of single-phased iron components [32].

As a concept-proof study, our work identified that the presence of a record high concentration of Li in Mg matrix (up to 14 wt%, equivalent to 40 at%) is favourable for slow and homogenous corrosion in a carbonated simulated body fluid, *i.e.* MEM, which is ascribed to the single-phase microstructure and formation of persistent Li_2CO_3 film in contact with MEM. The biocompatibility, mechanical degradation, and durability of the protective Li_2CO_3 film are of great significance for the validation of Mg-Li alloy systems in biomedical applications, which will be explored in our future work.

5. Conclusions

In this preliminary study, Mg alloy containing record high content of Li, Mg-14Li (wt%) was prepared and evaluated as a biodegradable material for future bone-fracture management, in comparison with a biocompatible Mg-0.5Zn-0.5Ca alloy and a commercial Mg alloy AZ31. The high content of Li dissolves completely in Mg matrix and leads to a single-phase (β-Li) microstructure. Such a unique microstructural feature gives rise to homogenous corrosion and the presence of high concentration of Li facilitates the formation of a protective film of Li_2CO_3, which contributes greatly to the low hydrogen evolution and mass loss rates of Mg-14Li specimens in MEM. In contrast, high corrosion kinetics and severely localised corrosion are apparent for Mg-0.5Zn-0.5Ca and AZ31 counterparts that exhibit heterogeneous microstructures and surfaces without the ability to form passive films in contact with carbonate-rich MEM. Such new findings could encourage the design and development of Mg components with controlled and predictable corrosion behaviour for next generation of biodegradable implants.

Acknowledgements

The authors gratefully acknowledge the financial support from the Australian Research Council (ARC) through Linkage scheme (LP150100343), microscopy facilities at Monash Centre for Electron Microscopy (MCEM), Monash University, and the XPS facilities, and the scientific and technical assistance, of the Australian Microscopy & Microanalysis Research Facility at RMIT University. C.L. is supported by China Scholarship Council (CSC).

References

[1] Y.F. Zheng, X.N. Gu, F. Witte, Biodegradable metals, Mater. Sci. Eng. R Rep. 77 (2014) 1–34.
[2] X.B. Chen, D.R. Nisbet, R.W. Li, P.N. Smith, T.B. Abbott, M.A. Easton, D.H. Zhang, N. Birbilis, Controlling initial biodegradation of magnesium by a biocompatible strontium phosphate conversion coating, Acta Biomater. 10 (3) (2014) 1463–1474.
[3] Y. Ding, C. Wen, P. Hodgson, Y. Li, Effects of alloying elements on the corrosion behavior and biocompatibility of biodegradable magnesium alloys: a review, J. Mater. Chem. B 2 (14) (2014) 1912–1933.
[4] H.X. Wang, S.K. Guan, X. Wang, C.X. Ren, L.G. Wang, *In vitro* degradation and mechanical integrity of Mg-Zn-Ca alloy coated with Ca-deficient hydroxyapatite by the pulse electrodeposition process, Acta Biomater. 6 (5) (2010) 1743–1748.
[5] S. Zhang, Y. Bi, J. Li, Z. Wang, J. Yan, J. Song, H. Sheng, H. Guo, Y. Li, Biodegradation behavior of magnesium and ZK60 alloy in artificial urine and rat models, Bioact. Mater. 2 (2) (2017) 53–62.
[6] J. Chen, L. Tan, K. Yang, Effect of heat treatment on mechanical and biodegradable properties of an extruded ZK60 alloy, Bioact. Mater. 2 (1) (2017) 19–26.
[7] S. Shadanbaz, G.J. Dias, Calcium phosphate coatings on magnesium alloys for biomedical applications: a review, Acta Biomater. 8 (1) (2012) 20–30.
[8] X.-B. Chen, N. Birbilis, T.B. Abbott, Review of corrosion-resistant conversion coatings for magnesium and its alloys, Corrosion 67 (3) (2011), 035005-1-035005-16.
[9] X.-B. Chen, N. Birbilis, T.B. Abbott, A simple route towards a hydroxyapatite-$Mg(OH)_2$ conversion coating for magnesium, Corros. Sci. 53 (6) (2011) 2263–2268.
[10] J. Tang, J. Wang, X. Xie, P. Zhang, Y. Lai, Y. Li, L. Qin, Surface coating reduces degradation rate of magnesium alloy developed for orthopaedic applications, J. Orthop. Trans. 1 (1) (2013) 41–48.
[11] X.-B. Chen, N.T. Kirkland, H. Krebs, M.A. Thiriat, S. Virtanen, D. Nisbet, N. Birbilis, Corrosion survey of Mg-*x*Ca and Mg-3Zn-*y*Ca alloys with and without calcium phosphate conversion coatings, Corros. Eng. Sci. Technol. 47 (5) (2012) 365–373.
[12] J.-L. Wang, S. Mukherjee, D.R. Nisbet, N. Birbilis, X.-B. Chen, In vitro evaluation of biodegradable magnesium alloys containing micro-alloying additions of strontium, with and without zinc, J. Mater. Chem. B 3 (45) (2015) 8874–8883.
[13] X.N. Gu, X.H. Xie, N. Li, Y.F. Zheng, L. Qin, In vitro and in vivo studies on a Mg-Sr binary alloy system developed as a new kind of biodegradable metal, Acta Biomater. 8 (6) (2012) 2360–2374.
[14] Y. Li, C. Wen, D. Mushahary, R. Sravanthi, N. Harishankar, G. Pande, P. Hodgson, Mg-Zr-Sr alloys as biodegradable implant materials, Acta Biomater. 8 (8) (2012) 3177–3188.
[15] S. Zhang, X. Zhang, C. Zhao, J. Li, Y. Song, C. Xie, H. Tao, Y. Zhang, Y. He, Y. Jiang, Y. Bian, Research on an Mg-Zn alloy as a degradable biomaterial, Acta Biomater. 6 (2) (2010) 626–640.
[16] P. Clément-Lacroix, M. Ai, F. Morvan, S. Roman-Roman, B. Vayssière, C. Belleville, K. Estrera, M.L. Warman, R. Baron, G. Rawadi, Lrp5-independent activation of Wnt signaling by lithium chloride increases bone formation and bone mass in mice, PNAS 102 (48) (2005) 17406–17411.
[17] A. Zamani, G.R. Omrani, M.M. Nasab, Lithium's effect on bone mineral density, Bone 44 (2) (2009) 331–334.
[18] M. Khorami, S. Hesaraki, A. Behnamghader, H. Nazarian, S. Shahrabi, *In vitro* bioactivity and biocompatibility of lithium substituted 45S5 bioglass, Mater. Sci. Eng. C 31 (7) (2011) 1584–1592.
[19] R. Wu, Y. Yan, G. Wang, L.E. Murr, W. Han, Z. Zhang, M. Zhang, Recent progress in magnesium-lithium alloys, Int. Mater. Rev. 60 (2) (2015) 65–100.
[20] C.Q. Li, D.K. Xu, S. Yu, L.Y. Sheng, E.H. Han, Effect of icosahedral phase on crystallographic texture and mechanical anisotropy of Mg-4%Li based alloys, J. Mater. Sci. Technol. 33 (5) (2017) 475–480.
[21] C.Q. Li, D.K. Xu, B.J. Wang, L.Y. Sheng, E.H. Han, Suppressing effect of heat treatment on the Portevin-Le Chatelier phenomenon of Mg-4%Li-6%Zn-1.2%Y alloy, J. Mater. Sci. Technol. 32 (12) (2016) 1232–1238.
[22] C.D. Yfantis, D.K. Yfantis, J. Anastassopoulou, T. Theophanides, M.P. Staiger, New magnesium alloys for bone tissue engineering: in vitro corrosion testing, WSEAS Trans. Environ. Dev. 2 (8) (2006) 1110–1115.
[23] W. Xu, N. Birbilis, G. Sha, Y. Wang, J.E. Daniels, Y. Xiao, M. Ferry, A high-specific-strength and corrosion-resistant magnesium alloy, Nat. Mater. 14 (12) (2015) 1229–1235.
[24] L. Hou, M. Raveggi, X.-B. Chen, W. Xu, K.J. Laws, Y. Wei, M. Ferry, N. Birbilis, Investigating the passivity and dissolution of a corrosion resistant Mg-33at.%Li alloy in aqueous chloride using online ICP-MS, J. Electrochem. Soc. 163 (6) (2016) C324–C329.
[25] ASTM, Standard Practice for Preparing, Cleaning, and Evaluating Corrosion Test Specimens, 2011.
[26] J.B. Clark, L. Zabdyr, Z. Moser, Phase Diagrams of Binary Magnesium Alloys, ASM International, Materials Park, OH, 2002.
[27] F. Witte, J. Fischer, J. Nellesen, H.-A. Crostack, V. Kaese, A. Pisch, F. Beckmann, H. Windhagen, *In vitro* and *in vivo* corrosion measurements of magnesium alloys, Biomater 27 (7) (2006) 1013–1018.
[28] L. Wang, T. Shinohara, B.-P. Zhang, Corrosion behavior of Mg, AZ31, and AZ91 alloys in dilute NaCl solutions, J. Solid State Electrochem 14 (10) (2010) 1897–1907.
[29] M.P. Staiger, A.M. Pietak, J. Huadmai, G. Dias, Magnesium and its alloys as orthopedic biomaterials: a review, Biomater 27 (9) (2006) 1728–1734.
[30] G.S. Frankel, N. Sridhar, Understanding localized corrosion, Mater. Today 11 (10) (2008) 38–44.
[31] R.-C. Zeng, L. Sun, Y.-F. Zheng, H.-Z. Cui, E.-H. Han, Corrosion and characterisation of dual phase Mg-Li-Ca alloy in Hank's solution: the influence of microstructural features, Corros. Sci. 79 (2014) 69–82.
[32] S. Li, L.H. Hihara, The comparison of the corrosion of ultrapure iron and low-carbon steel under NaCl-electrolyte droplets, Corros. Sci. 108 (2016) 200–204.